Chalcogenide Letters Vol. 17, No. 5, May 2020, p. 257 - 262

SOLVOTHERMAL SYNTHESIS OF Sb_2S_3 NEEDLES AND STUDY OF THE EFFECT OF THEIR INTERGROWTH ON THEIR OPTICAL PROPERTIES

O. E GUTIÉRREZ-GARZA[a], L. L. GARZA-TOVAR[a,*], E. QUIROGA-GONZÁLEZ[b], N. A. GARCÍA GÓMEZ[a], Y. PEÑA-MENDEZ[a], E. M. SÁNCHEZ CERVANTES[a]

[a]*Facultad de Ciencias Químicas, Universidad Autónoma de Nuevo León. Av. Universidad S/N, Cd. Universitaria. San Nicolás de los Garza, Nuevo León, 66455 México*

[b]*Institute of Physics, Benemérita Universidad Autónoma de Puebla. San Claudio and 18 Sur, Building IF-1, Ciudad Universitaria. 72570 Puebla, México*

Antimony trisulfide (Sb_2S_3) was successfully synthesized by the solvothermal route using either inorganic $SbCl_3$ or organic $C_8H_{10}K_2O_{15}Sb_2$ antimony precursors, and carbon disulfide as sulfur precursor with ethylene glycol as the solvent. The use of $SbCl_3$ resulted in single needles, while $C_8H_{10}K_2O_{15}Sb_2$ conducted to needle-bundles. In both cases, the crystal structure is orthorhombic (Stibnite), as a single phase. The introduction of structural defects caused by the intergrowth is evidenced by Raman spectroscopy. The defects originate a variation of the optical bandgap of the material.

(Received January 12, 2020; Accepted May 14, 2020)

Keywords: Chalcogenides, Sb_2S_3 needles, Engineering of defects, Raman spectroscopy, Optical properties

1. Introduction

Sb_2S_3 is a semiconductor material that has attracted attention for different applications, like photosensors [1] and thermoelectric devices [2], due to its suitable optical and electrical properties that can be enhanced synthesizing the material in 1D or 2D. 1D nanostructures of Sb_2S_3 such as nanorods, nanowires, microtubes and nanobelts are common, since the material usually grows anisotropically in the axial direction. Such structures can be obtained by using different synthetic methods: thermal evaporation at high vacuum [3], spray pyrolysis [4], precipitation [5], ionic liquid assisted ultrasonic bath [6], sonochemistry [7], colloidal [8], hydrothermal [9, 10] and solvothermal [11]. The simplest technique is the hydro- or solvo-thermal synthesis, which additionally it is very powerful for obtaining crystals of good quality with even atypical morphologies. Chen *et al.* reported the synthesis of wires using the hydrothermal method. They obtained wires of about 5–20 μm in length and 300–500 nm in diameter. The formation of thin rods was attributed to the separation of an individual thick rod and subsequent growth along the preferential direction inherent to the stratified structure of Sb_2S_3 [10]. Alemi *et al.* reported the synthesis of Sb_2S_3 wires by hydrothermal synthesis, obtaining wires with a length of 6 μm and diameter of 30-160 nm [12]. Xu et al. reported the synthesis of Sb_2S_3 by solvothermal synthesis. Wires with dimensions of 20 μm x 500 nm were obtained [13]. Kavinchan *et al.* obtained flower-like structures by means of a solvothermal process. Spherical structures of about ~8 μm in diameter, consisting of fine wires, have also been obtained [14]. Lu *et al.* reported the synthesis of Sb_2S_3 bars by the hydrothermal route attaining bars of 5 μm in length that were coupled in different directions [15]. As mentioned before, there is a variety of reports of Sb_2S_3 1D structures. In the same form, there is also a wide range of reported optical bandgaps for those structures. In general, the optical bandgap for Sb_2S_3 ranges from about 1.4 to 1.8 eV [16, 17]. However, not much has been discussed about the origin of that big difference, besides quantum confinement and

* Corresponding author lorena.garzatv@uanl.edu.mx

excitonic effects (for particles with dimensions in the range of the Bohr Radius) and stoichiometry changes, even dealing with intergrowth needles [18]. In this work we report the synthesis of Sb_2S_3 single and interconnected needles by solvothermal method, using different Sb starting materials, evaluating the effect of the intergrowth in their optical properties.

2. Experimental section

2.1. Synthesis

3 mM of antimony chloride, $SbCl_3$ (Sigma Aldrich 99%), or antimony potassium tartrate hydrate, $C_8H_{10}K_2O_{15}Sb_2 \cdot 3H_2O$ named from now on as SbKT (Alfa Aesar 98%), were weighted inside a glove box to avoid their reaction with water. They were mixed with 15 mL of ethylene glycol, EG (Sigma Aldrich 99.5%), and 80 µL of carbon disulfide, CS_2 (Sigma Aldrich 99.5%), in a beaker. The mixture was transferred to a solvothermal reactor, which was placed in an oven at a temperature of 180 °C for 24 h. After the thermal treatment, the reactor was left to cool down at room temperature. The solid reaction products were separated from the mother solution by centrifugation and were washed three times with ethanol. The solid products were then dried at 80 °C in a vacuum oven.

2.2. Powder X-ray diffraction measurements

The crystals obtained from each reaction were placed over zero background sample holders to run x-ray diffraction analysis. Samples were analyzed at room temperature on a Bruker D2 Phaser powder diffractometer, using Cu-Kα radiation (λ = 1.5418 Å) with 30kV and 10 mA and lynx-eye detector, in the range of $5 < 2\theta < 90^o$ with a step size of 0.05º and step time of 0.5 s. Crystalline phases present were identified using the PDF-2 database and the crystal size of Sb_2S_3 was determined using the Scherrer equation.

2.3. SEM analysis

Crystals morphology and size were evaluated by scanning electron microscopy (SEM) using a JEOL JCM-6000 (15 kV).

2.4. Raman spectroscopy measurements

Raman spectra were carried out using a Thermo Scientific DXR Raman spectrometer with a laser of 785 nm coupled to an Olympus U-TV0.5XC-3 microscope. Samples were analyzed at room temperature with a laser spot of 50 µm and laser power of 6W.

2.5. Optical properties UV-Vis

Optical properties were carried out using a UV-Vis Evolution 300 Thermo Scientific apparatus. A 100% reflectance standard of $BaSO_4$ was used to analyze the samples. Reflectance spectra were measured for each material, expressing the intensity in %. The optical bandgap Eg was calculated using the Kubelka-Munk function $\alpha/s = (1-R)^2/2R$.

3. Results and discussion

The x-ray powder diffractograms obtained from the reaction products for the synthesis of Sb_2S_3 are presented in Figure 1. Crystalline phase identification confirms the presence of Sb_2S_3 with orthorhombic structure according to the PDF file 042-1393. No secondary phases were detected, indicating that experimental conditions for the two samples favor the formation of a single phase. Diffraction peaks show relatively high intensity originated from crystallographic planes with Miller indexes (120), (130) and (240). This suggests that crystal growth is preferably along the (010) direction, which is in agreement with one dimensional growth of structures comparably to the work reported by Xinyu *et al.* [19].

SEM images and particle diameter size histograms of the samples are shown in Figure 2. As can be seen, Sb_2S_3 obtained with inorganic precursor crystalizes as long needles. Some of the needles are isolated, and some of them grow together with a celery-kind morphology with length 40-60 μm and width 200-1400 nm. Typically, groups of 4 needles grow together. The needles average diameter of 730 nm ± 157 nm (standard deviation) was observed. Although it is well known that EG acts as capping agent to obtain nanoparticles, in this work it is acting as solvent and dispersive medium for the starting materials, playing an important role in the nucleation and growth of Sb_2S_3 micro needles.

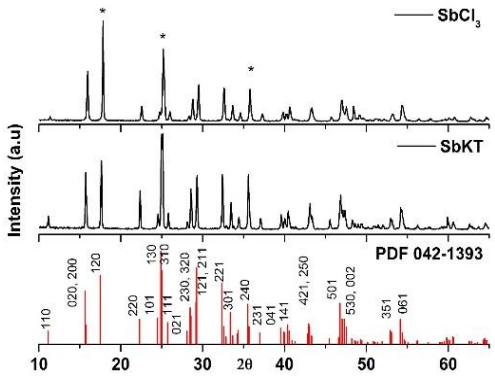

Fig. 1. Diffractograms of samples prepared with $SbCl_3$ and SbKT.
(peaks indicating preferential orientation).*

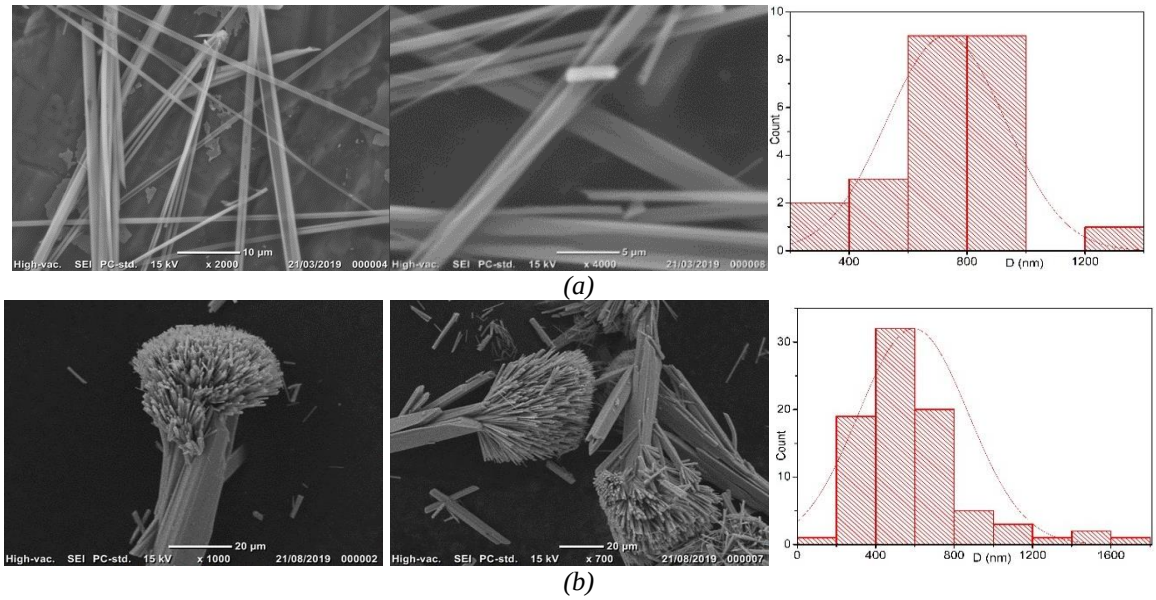

Fig. 2. SEM images and size histograms of Sb_2S_3 prepared with (a) $SbCl_3$ and (b) SbKT.

On the other hand, the Sb_2S_3 obtained using the organic precursor, presents completely different morphology. The structure formed from a large branch of about 60-90 μm length x 8-13 μm width and a bouquet of smaller branches (hundreds of them) in one end with length between 10 – 30 μm and width of 200-1800 nm. Smaller branches average diameter of 607 nm ± 201 nm (standard deviation) was also observed. The employment of tartrate precursor affects the hierarchical growth. Due to its structure, this sample can be considered with a high number of structural defects.

Figure 3 shows the Raman spectra of the samples. The band assignment is presented in Table 1, and agrees with previous reports on Sb_2S_3 [20, 21, 22]. It is important to mention that there are two different positions of Sb in the structure of stibnite, with different coordination to S. It is possible to observe Raman modes related to every of those Sb atoms, which are indicated in the table as Sb(1) and Sb(2).

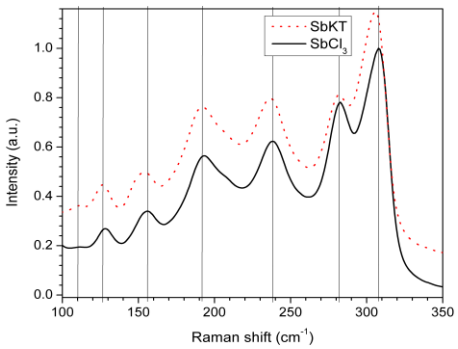

Fig. 3. Raman spectrum of Sb_2S_3 prepared with $SbCl_3$ and SbKT.

Table 1. Assignment of the Raman bands of the samples prepared with $SbCl_3$ and SbKT [22].

Band position, cm^{-1}	Origin
110	S-Sb(1)-S symmetric bending
126	S-Sb(1)-S asymmetric bending
156	S-Sb(1)-S symmetric stretching
192	S-Sb(2)-S symmetric bending
238	S-Sb(2)-S asymmetric bending
282	S-Sb(2)-S symmetric stretching
308	S-Sb(2)-S symmetric stretching, short Sb-S

Compared to the Raman spectra reported for thin films of Sb_2S_3, in the present work the most intense band is the one at about 307 cm^{-1}, instead of the one at about 281 cm^{-1}; this difference in intensity can be attributed to differences in particle morphology: the crystals of the present report are 1D, as previously indicated with SEM. On the other hand, it is important to notice that there is a red shift in the positions of some peaks of the sample prepared with SbKT compared with the spectrum of the sample prepared with $SbCl_3$. It is reported that the peaks related to symmetric stretching are more sensitive to stress [22]. In that report, applying a compressive stress, a blue-shift of the Raman band at 156 cm^{-1} is obtained. As a red shift is observed in the present work, the stress must be tensile. That tensile stress could be caused by the large number of structural defects of the sample prepared with SbKT and is mostly observable for shorter Sb-S bonds.

A Kubelka-Munk plot for the determination of the optical bandgap of the different samples is shown in Figure 4. From the absorption edge it is been confirmed that the Sb_2S_3 has a direct band gap. The estimated band gap value for the sample prepared with the organic precursor is 1.415, and for the sample prepared with inorganic precursor is of 1.445. These values are relatively close to those read from UV-vis plots of other reports of Sb_2S_3 needles, of about 1.6 eV [1, 18].

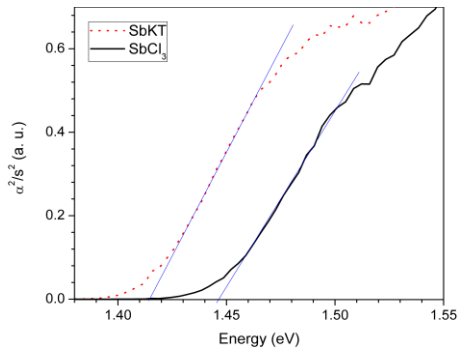

Fig. 4. Kubelka-Munk plot for Sb_2S_3 prepared with $SbCl_3$ and SbKT.

Quasiparticle calculations of the band structure of Sb_2S_3 indicate a bandgap of 1.54 eV [17], value that coincides with the one obtained for stoichiometric annealed thin films of this material [16]. The red shift of the present samples may be due to the structural defects. The sample with more intergrown needles, and thus more structural defects (sample prepared with SbKT), presents the lowest bandgap. This agrees with a study of Ag_2Se nanocrystals, where their photoluminescence suffered a red shift when the number of defects (dislocations) increased [23].

4. Conclusions

Sb_2S_3 with either wire (1D) or branched (3D) structure has been successfully synthesized via solvothermal route from inorganic $SbCl_3$ and organic SbKT precursors with CS_2 as sulfur source and EG as solvent under 180°C for 24 h, filling the reactor to 25%. The optical bandgap was of 1.415 and 1.445 eV for the samples prepared with SbKT and $SbCl_3$ respectively. The lower bandgap of the sample prepared with SbKT is an indication of the higher number of structural defects, as confirmed by Raman spectroscopy, where a red shift was obtained in the stretching modes of that sample compared with the ones of the other sample. This work represents the first directed attempt to modify the bandgap of Sb_2S_3 by modifying the number of structural defects. Bringing the bandgap to the range of 1.5 eV may increase its suitability as absorber material in solar cells or photodetectors working in the visible light region.

Acknowledgements

This work was supported by SEP-CONACYT (Mexico) through research project numbers CB-2012-01 ref. 189865 and PAICYT-UANL project number IT1056-19.

References

[1] J. Chao, B. Liang, X. Hou, Z. Liu, Z. Xie, B. Liu, G. Shen, Opt Express **21**(11), 13639 (2013).
[2] M. Telkes, Am. Mineral. **35**(7-8), 536 (1950).
[3] R. G. Sotelo Marquina, T. G. Sanchez, N. R. Mathews, X. Mathew, Mater. Res. Bull. **90**, 285 (2017).
[4] K. Y. Rajpure, C. H. Bhosale, Mater. Chem. Phys. **73**(1), 6 (2002).
[5] Q. Wei, N. Pi, Y. Huang, Y. Yang, Y. Liu, P. Yao, MATEC Web Conf. **67**, 01008 (2016).
[6] P. Salinas-Estevané, E. M. Sánchez, Cryst. Growth Des. **10**(9), 3917 (2010).
[7] H. Wang, Y. N. Lu, J. J. Zhu, H.Y. Chen, Inorg. Chem. **42**(20), 6404 (2003).
[8] I. L. Validžić, M. Mitrić, Mater. Lett. **65**(12), 1919 (2011).
[9] L. Wu, H. Xu, Q. Han, X. Wang, J. Alloys Compd. **572**, 56 (2013).

[10] G. Y. Chen, W. X. Zhang, A. W. Xu, Mater. Chem. Phys. **123**(1), 236 (2010).
[11] H. Zhang, C. Hu, Y. Ding, Y. Lin, J. Alloys Compd. **625**, 90 (2015).
[12] A. Alemi, Y. Hanifehpour, S. W. Joo, J. Nanomater. **2011**, 46 (2011).
[13] Y. Xu, Z. Ren, G. Cao, W. Ren, K. Deng, Y. Zhong, Cryst. Res. Technol. **44**(8), 851 (2009).
[14] J. Kavinchan, T. Thongtem, S. Thongtem, E. Saksornchai, J. Nanomater. **2013**, 4. (2013).
[15] Q. Lu, H. Zeng, Z. Wang, X. Cao, L. Zhang, Nanotechnology **17**(9), 2098 (2006).
[16] S. Mahanty, J. M. Merino, M. Leon, J. Vac. Sci. Technol. A **15**(6), 3060 (1997).
[17] M. R. Filip, C. E. Patrick, F. Giustino, Physical Review B **87**(20), 205125 (2013).
[18] I. L. Validžić, M. Mitrić, N. D. Abazović, B. M Jokić, A. S. Milošević, Z. S. Popović, F. R. Vukajlović, Semicond Sci Tech. **29**(3), 035007(2014).
[19] Y. Xinyu, Z. Jiasong, L. Lijun, L. Xiaojuan, L. Haitao, X. Weidong, Mater. Chem. Phys. **118**(2-3), 432 (2009).
[20] M. I. Medina-Montes, Z. Montiel-González, N. R. Mathews, X. Mathew, J. Phys. Chem. Solids **111**, 182 (2017).
[21] M. I. Medina-Montes, Z. Montiel-González, F. Paraguay-Delgado, N.R. Mathews, X. Mathew, J. Mater. Sci.-Mater. E **27**(9), 9710 (2016).
[22] I. Efthimiopoulos, C. Buchan, Y. Wang, Sci. Rep. UK **6**, 24246 (2016).
[23] Q. Cao, Cheng, Y. F. Bi, H. Zhao, X. Yuan, K. Liu, Q. Che, R. J. Mater. Chem. A **3**(40), 20051 (2015).